Composite Structures xxx (2018) xxx-xxx

Contents lists available at ScienceDirect

Composite Structures

journal homepage: www.elsevier.com

# Effect of using CFRP wraps on the strength and ductility behaviors of exterior reinforced concrete joint

Yazan B. Abu Tahnat, Mahmud M.S. Dwaikat, Mohammad A. Samaaneh*

*Department of Civil Engineering, An-Najah National University, Nablus, Palestine*

ARTICLE INFO

*Keywords:*
Fiber-Reinforced Polymer (FRP)
Ductility
Reinforced concrete joints
Finite Element modeling
ABAQUS
Design guidelines

ABSTRACT

One considerable weakness in reinforced concrete (R.C) structures is the connection between beams and columns. Several researchers showed that R.C joints suffer brittle failure due to combined effect of loading on the joints. Therefore, the ductility of the beam-column joints in R.C structures is an essential factor to prevent sudden failure of the joint. Different techniques were adapted by several researchers to increase the ductility and strength of beam-column joints including the use of high strength concrete, special stirrups and reinforcement configuration, steel plates and Fiber-Reinforced Polymer (FRP).

One way to improve the ductility of such joints is the use of FRP sheet wraps. This research focuses on studying the effect of using FRP wraps around beam on ductility of exterior R.C beam-column joints. To achieve this main objective; this research focuses on the key parameters controlling ductility of joints, namely, relative inertia of column to beam (G), amount of transverse steel in joint $(Av/s)_J$ and amount of transverse steel in beam $(Av/s)_B$. Finite Element (F.E.) analysis using commercial F.E. software (ABAQUS) is used to investigate the ductility behavior of R.C joints strengthened by FRP. The mentioned parameters are investigated numerically. Results show that the using CFRP wraps around beam converts the brittle failure to ductile failure. Stirrups continuity inside the joint increases the capacity and ductility for models dominated by shear failure.

## 1. Introduction

Maintaining minimum ductility of beam-column joints in R.C structures is essential to prevent sudden failure of such joints which severely affects all the structure. In typical structures, different types of framed joints exist such as; corner-roof joint, corner joint, exterior-roof joint, exterior joint, and interior joint as shown in Fig. 1.

Each type of these joints undergoes different kind of behavior due to differences in combination of internal stresses acting on the joint. As shear and flexural stresses act simultaneously in a complex combination within the joint region, these stresses cause an internal diagonal tensile and compressive stresses. If the diagonal stress is exceeding concrete capacity, it would lead to diagonal cracking (in tension) or crushing (in compression) of the concrete as shown in Fig. 2 [1]. Therefore, strengthening techniques and reinforcement detailing can vary depending on the expected behavior of each type of joints.

Extensive studies were conducted to investigate the behavior of beam-column joints. Kaliluthin et al. [2] and Uma and Prasad [3] showed that R.C joints suffer brittle failure due to the combined effect of loading on the joints.

Many strengthening techniques were used to improve the behavior of each type of joints, such as using steel jacketing [4], improving the detailing of the R.C joint [5]. Recently, the use of Fiber Reinforced Polymer (FRP) composites presented an effective technique for strengthening and rehabilitation of concrete structures. Different methods of retrofitting R.C joints using FRP are available; sheets, laminates, strips or rebar. Ghobarah and Said [6] experimentally tested two full-scale specimens of exterior R.C beam column joint to study the effect of GFRP sheets on the behavior of joint. Results showed that using GFRP within the joint leads to increase the ductility by 60%. El-Amoury [7] tested four full scale specimens to study the effect of GFRP and CFRP sheets on the ductility of exterior R.C beam-column joints. The results showed that the retrofitted specimens behave more ductile than the un-retrofitted control specimen. Mahmoud et al. [8] conducted experimen-

* Corresponding author.
*Email address:* m.samaaneh@najah.edu (M.A. Samaaneh)

https://doi.org/10.1016/j.compstruct.2018.06.082
Received 28 March 2018; Received in revised form 4 June 2018; Accepted 21 June 2018
Available online xxx

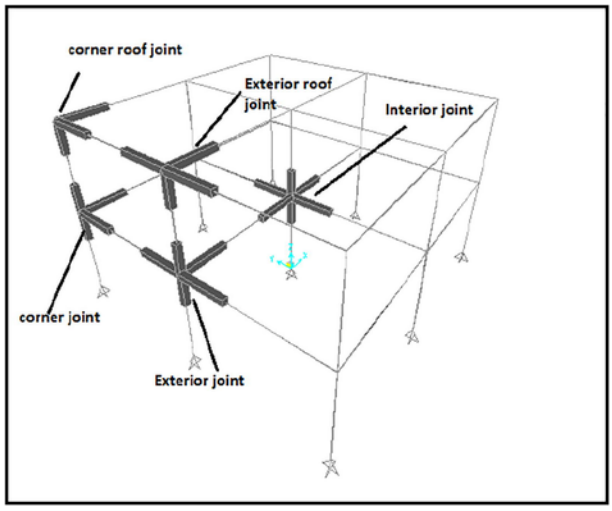


**Fig. 1.** Types of joints.

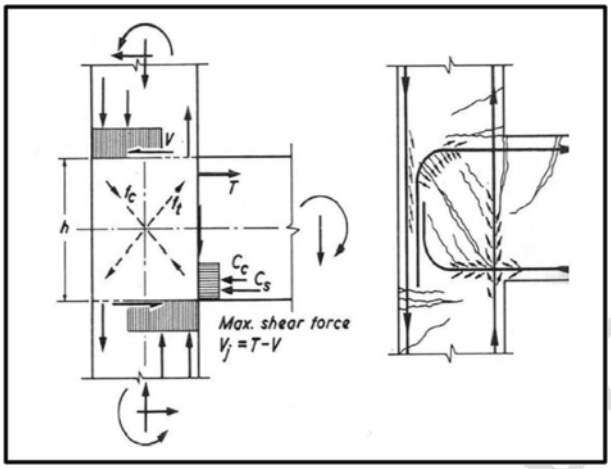


**Fig. 2.** Forces acting on exterior R.C joint [1].

tal testing on a total of 10 half-scale specimens of exterior R.C beam-column joints to study the effect of retrofitting techniques on the strength and ductility if exterior R.C beam-column joints. Results showed that using either CFRP fabric sheets or plates as strengthening material enhanced efficiently the failure characteristics of the defected beam–column joints if the proper configuration was chosen. Also, using CFRP as a strengthening material led to increase the ultimate capacity.

Numerical investigation of ability of CFRP sheets to maintain the composite action at the negative moment region for continuous composite girder was studied by Samaaneh et al. [9]. Results showed that the girder capacity and stiffness increase with the use of CFRP sheets bonded to the top of the concrete slab at the negative moment region. The increase in ultimate capacity is directly proportional to CFRP thickness up to certain thickness, when the negative moment capacity is close to the positive moment capacity. Numerical analysis of exterior R.C beam-column joint was conducted by Bidgar and Bhattacharya [10], and showed that the axial load on column made a slight increase in the beam resisting moment capacity.

Clyde et al. [11] conducted experimental testing on a total of 4 half-scale specimens of exterior R.C beam-column joints to study the effect of axial force on the column. Results showed that there a slight increase in the sustained peak lateral load for each specimen. On the other hand, there is a distinct difference in ductility. The specimens with the lower axial load were 50% more ductile than the beam-column joints with higher axial load.

Based on the literature, there is a limited work conducted to quantify the ductility of R.C beam-column joint strengthened by CFRP. This research focuses on defining the ductility behavior of such joint subjected to constant axial load combined with moment. Four main parameters are investigated numerically (Relative inertia of column relative to beam (G), shear reinforcement in joint $(Av/s)_J$, shear reinforcement in beam $(Av/s)_B$, and the effect of CFRP).

## 2. Modeling and verification

Numerical investigation of structures offers an attractive technique of research due to low cost, quick results and ability to study several variables in depth. Therefore, a three-dimensional (3-D) non-linear F.E. joint model is built using commercial software ABAQUS [12]. The details and development of the F.E. model is outlined by Abu-Tahnat [13]. A brief description of these details is mentioned here for the sake of completeness.

### 2.1. Loading steps and boundary conditions

Pseudo-dynamic analysis is utilized to obtain the full behavior and to avoid convergence problem in ABAQUS. Therefore, load is applied with large time steps in order to converge to the static solution. Using the dynamic analysis is used instead of static analysis to help convergence of highly non-linear behavior of cohesive contact in ABAQUS.

Schematic view of the F.E. model, boundary conditions and loading sequences for the model are shown in Fig. 3. The top end of the column is restrained by a rigid surface allowing the end to behave as pin,

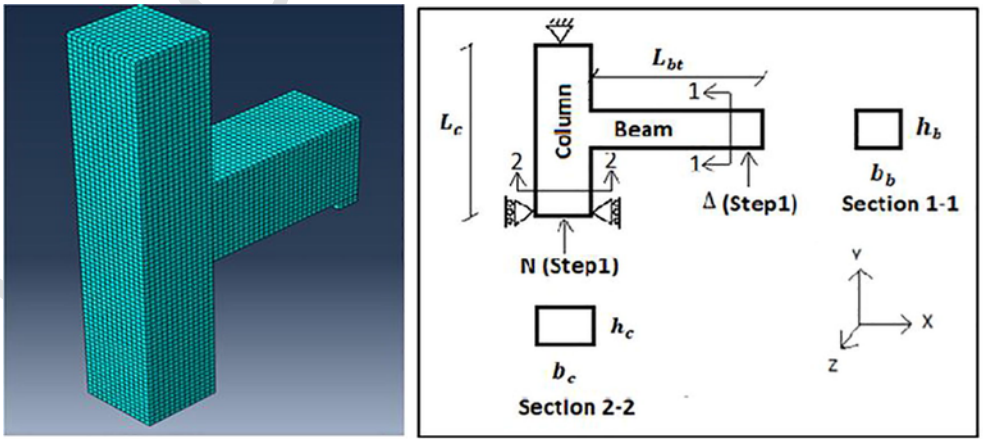


**Fig. 3.** F.E. model and location of loads and boundary conditions.

in addition the bottom end is restrained by a rigid surface allowing the end to behave as roller in the Y-direction. It should be noted that these rigid surfaces restrain the in-plane movement of the column ends. Such restraint conditions are generally assumed for similar cases in the literature [14]. A constant axial load (as reported in experimental tests) is initially applied on column. This is followed by an incremental load applied at tip of beam as displacement control.

### 2.2. Modeling of interfaces

Different contact models are used to model the interfacial region depending on the actual behavior and degree of accuracy. Tie contact is used between parts of beam and column. This type of contact is also used between loading plate and beam. This contact considers perfect bond between two surfaces to make the translational and rotational motion as well as all other active degrees of freedom equal for a pair of surfaces. At the same time, the contact between reinforcement and concrete is assumed to be perfectly bonded surfaces with no slip. This is justified by the enough development length of rebar and available friction between them, so embedded region contact is used to simulate the perfect bond. Cohesive contact is used to simulate the behavior of adhesive material between concrete and CFRP as will be discussed later. This contact can be used to model the delamination and slip at interfaces directly interns of traction versus separation.

Both separation-traction and force-slip constitutive curves are needed to model the cohesive behavior. Many models exist with various degrees of complexity. The linear-brittle model, developed by Neubauer and Rostasy [15] is used to model the cohesive contact as shown in Fig. 4 with initial shear stiffness ($K_0$) and shear strength ($t_{max}$) as proposed by Obaidat et al. [16] as shown in Eqs. (1) and (2). It must be noticed that there is a premature failure of cohesive contact in this model, so to prevent the convergence problems in ABAQUS, the descending branch is assumed linear with small slip after maximum slip ($S_f$). However, the maximum normal strength can be considered to be equal tensile strength of concrete [16]. On the other hand, normal stiffness is assumed equal to shear stiffness as no sufficient data about it. The verified experimental beam-column joints had not reported any de-bonding of FRP. Same assumptions are extended to the current work as adequate development length and sheeting wraps are provided.

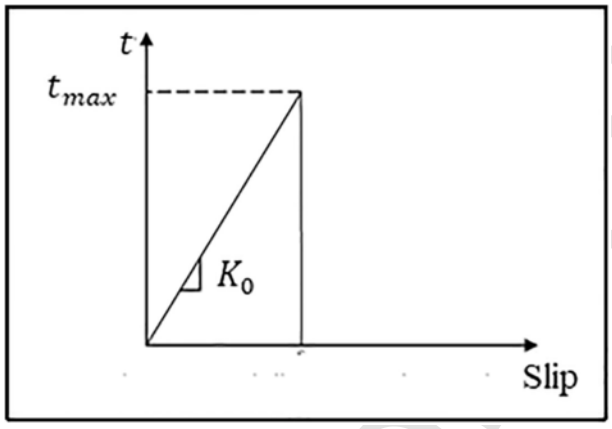


**Fig. 4.** Bond-slip curve model [15].

$$K_0 = 0.16\frac{G_a}{t_a} + 0.47 \tag{1}$$

$$t_{\max} = 1.46 G_a^{0.165} f_{ct}^{1.033} \tag{2}$$

where:

$K_0$: Initial shear stiffness (GPa)
$G_a$: Shear modulus of adhesive (GPa)
$t_a$: Adhesive thickness (mm)
$f_{ct}$: Tensile strength of concrete (MPa)
$t_{max}$: Shear strength for cohesive interaction (MPa).

### 2.3. Meshing type and sensitivity study

The components of beam-column joint are meshed individually using part-by-part basis instead of using global or sweep mesh. Eight-noded linear brick element (C3D8R) is used to model the solid elements; concrete and loading plate. A 2-node linear 3-D truss element is used to model main and transfers reinforcement (T3D2), whereas 4-noded shell element (S4R) used to model CFRP as shown in Fig. 5.

Sensitivity study are conducted to eliminate the effect of mesh size on accuracy of results, Mesh size of 15 mm is adapted for all models

### 2.4. Verification of model

The numerical model is validated using experimental results from literature. Many experiments concerning R.C beam-column joints were reported in literature. However, many of them were not described in detailed. A set of clearly reported experiments are selected to validate the F.E. results. Total of seven independent reported tests were used to establish the verification. One of them is an exterior R.C beam-column joint, without CFRP strengthening, subjected to cyclic loading (displacement control) which was tested by Clyde et al. [11] with dimen-

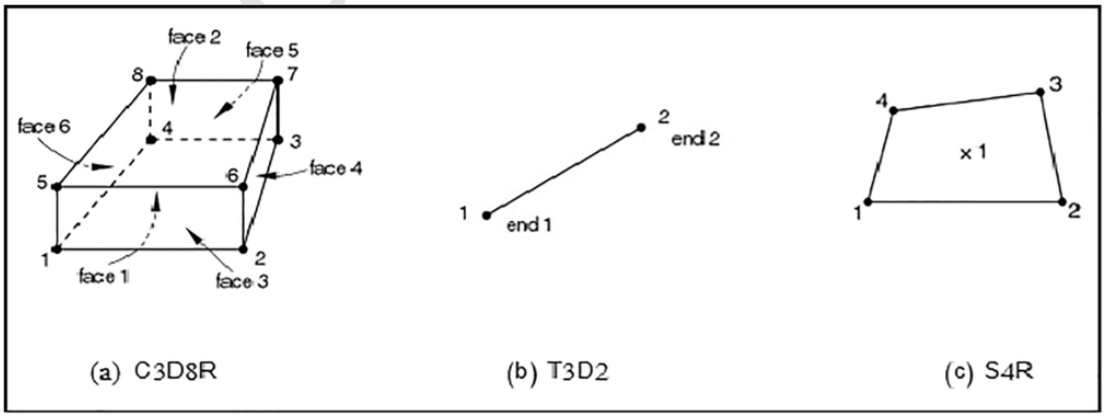


**Fig. 5.** F.E. Mesh Type.

sions and reinforcement detailing as shown in Fig. 6. In addition, three of the exterior R.C beam-column joints were tested monotonically (load control) by Mahmoud et al. [8], two of them without FRP named J0 and JI0 while third specimen, named JI1, with strengthening configuration represented two perpendicular overlaying fabric sheets on the beam–column joint. One layer of 200 mm width and 1000 mm length parallel to the column axis was bonded to each side of the column. Then a horizontal U-shaped layer of 200 mm width and extended by 600 mm length parallel to the beam axis was bonded to each side. Finally, three 100 mm in width U-shaped sheets were used at the joint in order to prevent the premature peeling of the sheets at the beam-column joint. The dimensions and reinforcement detailing for these joints are shown in Fig. 7a and b. The remaining three are the exterior R.C beam-column joints subjected to cyclic displacement and tested by El-Amory [7] with dimensions and reinforcement detailing as shown in Fig. 8. One of them without FRP named T-S1, while the second and third specimens with adding CFRP and GFRP sheets which are named T-S4R and T-S5 respectively. Fig. 9a and b illustrate the strengthening techniques of specimens T-S4R and T-S5 respectively.

*2.4.1. Material modeling*

In this section, constitutive models for concrete and steel under compression and tension loads are presented. A constitutive model for FRP lamina is included too.

*2.4.1.1. Modeling of concrete* Concrete damage plasticity (CDP) model is used to model the complex nonlinear behavior of concrete. In this model, two main failure criteria are considered; tensile cracking and compressive crushing of the concrete material. Compression and tension behavior of concrete under uniaxial loading is shown in Fig. 10.

CDP model allows capturing of strength and stiffness degradation through tension and compression damages parameters ($d_t$, $d_c$, respectively) of concrete as shown in Fig. 10 [17].

As shown in Fig. 10, the unloaded response of concrete specimen is weakened because the elastic stiffness of the material is damaged or degraded due to cracks. The degradation of the elastic stiffness on the strain softening branch of the stress-strain curve is characterized by two damage variables, $d_t$ and $d_c$, which can take values from zero to one. Zero represents the undamaged material where one represents total loss of strength. However, Wahalathantri et al. [18] defined $d_c$ as the ratio between the inelastic strain (crushing strain) and total strain, and $d_t$ is defined as the ratio between the cracking strain and total strain. $E_0$ is the initial (undamaged) elastic stiffness of the material and are compressive plastic strain, tensile plastic strain, compressive inelastic strain and tensile inelastic strain respectively. The elastic relations under uniaxial tension ($\sigma_t$) and compression ($\sigma_c$) are taken into account in Eqs. (3) and (4), respectively.

$$\sigma_t = (1 - d_t)\cdot E_0 \cdot (\varepsilon_t - \tilde{\varepsilon}_t^{pl}) \tag{3}$$

$$\sigma_c = (1 - d_c)\cdot E_0 \cdot (\varepsilon_c - \tilde{\varepsilon}_c^{pl}) \tag{4}$$

where the effective tensile and compressive cohesion stress which are used to determine the yield point according to the yield function. The model makes use of the yield function according to Lubliner et al. [19] with the modifications proposed by Lee and Fenves [20] to account for different evolution of strength under tension and compression under multi-axial loading case. Therefore, the material model captures the confinement effect that results from tri-axial stress data in concrete al-

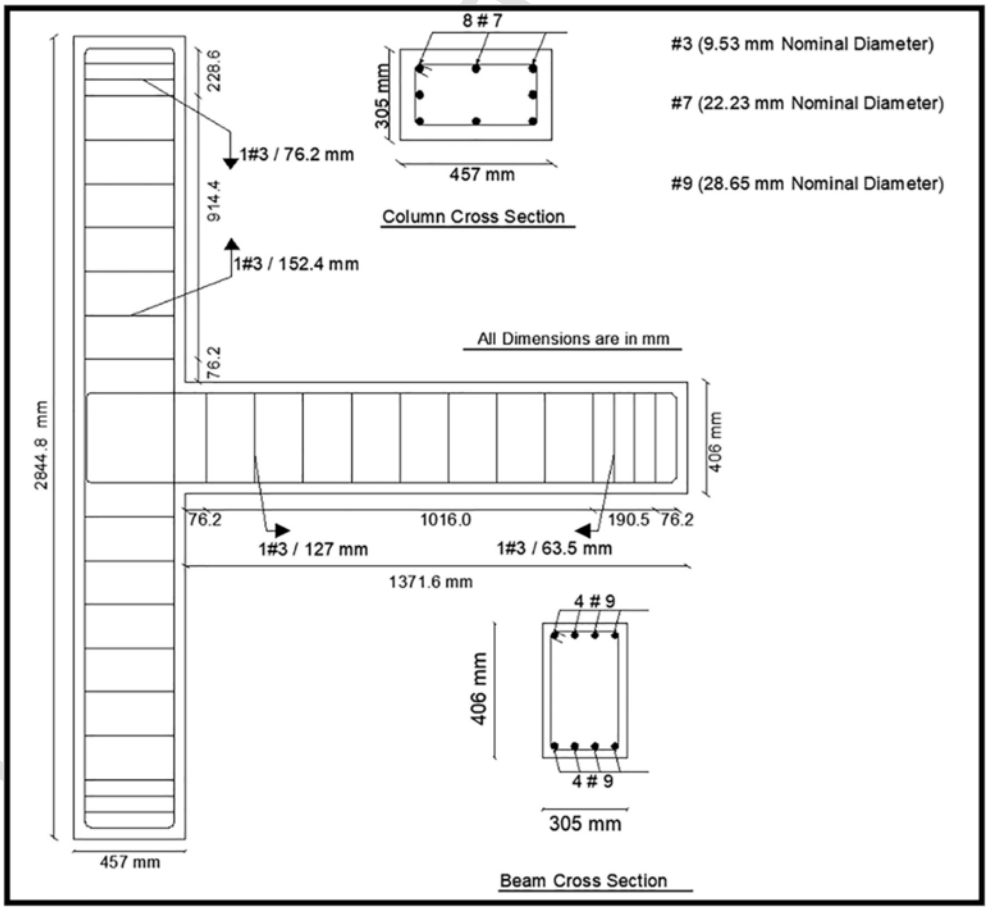


**Fig. 6.** Dimensions and reinforcement details for the exterior R.C beam-column joint (Test#2) [11].

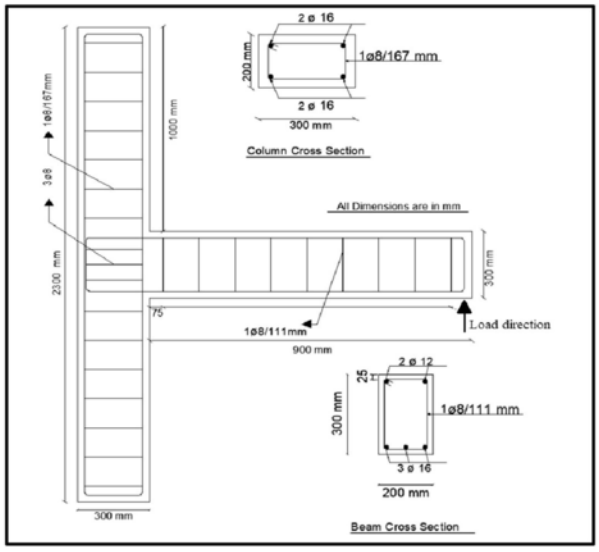


(a) Joint J0

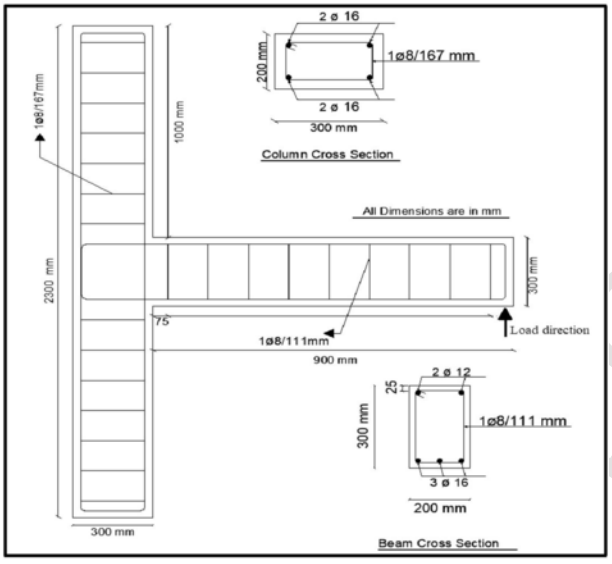


(b) Joints JI0 and JI1

**Fig. 7.** Dimensions and reinforcement details for joints J0, JI0 and JI1 [8].

lowing improvement of compressive capacity in the case of hydrostatic stress state.

.*Uniaxial compressive behavior* Generally, many researchers suggested equations that describe the behavior of concrete under uniaxial compression stress. However, most of these equations, including the models suggested by Mander et al. [21] and Yong et al. [22], do not describe full stress-strain curve of concrete. For this reason, the stress-strain equation proposed by Saenz [23] and validated by Asran et al. [24] is used to define full behavior of concrete under uniaxial compressive stress as shown in Eqs. (5)–(11).

$$\sigma_c = \frac{E_c \varepsilon_c}{1 + (R + R_E - 2)\frac{\varepsilon_c}{\varepsilon_0} - (2R - 1)\left(\frac{\varepsilon_c}{\varepsilon_0}\right)^2 + R\left(\frac{\varepsilon_c}{\varepsilon_0}\right)^3} \quad (5)$$

$$E_c = 4700\sqrt{f'_c} \quad (6)$$

$$R = \frac{R_E(R_\sigma - 1)}{(R_\varepsilon - 1)^2} - \frac{1}{R_\varepsilon} \quad (7)$$

$$R_E = \frac{E_c}{E_0} \quad (8)$$

$$R_\sigma = \frac{f_c}{\sigma_f} \quad (9)$$

$$R_\varepsilon = \frac{\varepsilon_f}{\varepsilon_0} \quad (10)$$

$$E_0 = \frac{f_c}{\varepsilon_0} \quad (11)$$

where:

$\sigma_c$: Concrete compressive stress (MPa)
$E_c$:Modulus of elasticity of concrete (MPa)
$E_0$: Secant modulus of concrete (MPa)
$f'_c$: Maximum compressive strength of concrete (MPa)
$\varepsilon_c$: Compression strain
$\varepsilon_0$: Strain corresponding to $f'_c$ which is equal approximately 0.0025 as reported by Hu and Schnobrich [25].
$\varepsilon_f$: Maximum strain.
$\sigma_f$: Stress at maximum strain (MPa).
$R$: Ratio relation
$R_E$: Modular ratio.
$R_\sigma$: Stress ratio, which is equal 4 as reported by Hu and Schnobrich [25].
$R_\varepsilon$: Strain ratio, which is equal 4 as reported by Hu and Schnobrich [25].

.*Tension behavior* The stress-strain curve for concrete under tension is tested experimentally by Sharif et al. [26] for concrete of compressive strength 25 MPa. The maximum tensile stress was reported as 2.9 MPa corresponding to modulus of rupture of concrete which is equal $0.62\sqrt{f'_c}$ according to ACI 318 [27], and maximum strain is 0.003. Asran et al. [24] used this method to define tension behavior of concrete in ABAQUS and got acceptable results in their verification.

Concrete modeling according to CDP is based on many parameters as summarized in Table 1. Default values of those parameters are indicated in ABAQUS User's Manual [17].

Table 2 shows the compressive strength, elastic modulus and Poisson's ratio of concrete for all joints that used in verification. Fig. 11a shows the uniaxial compression stress-inelastic strain curve of concrete, while Fig. 11b shows the tension stress-cracking strain curve of concrete. Also, Fig. 11c shows the compression damage parameter versus inelastic strain curve, while Fig. 11d shows the tension damage parameter versus cracking strain curve.

*2.4.1.2. Modeling of steel* An isotropic behavior was used to model the reinforcement and loading plate. This mean that the yield surface changes size uniformly in all directions such that the yield stress in-

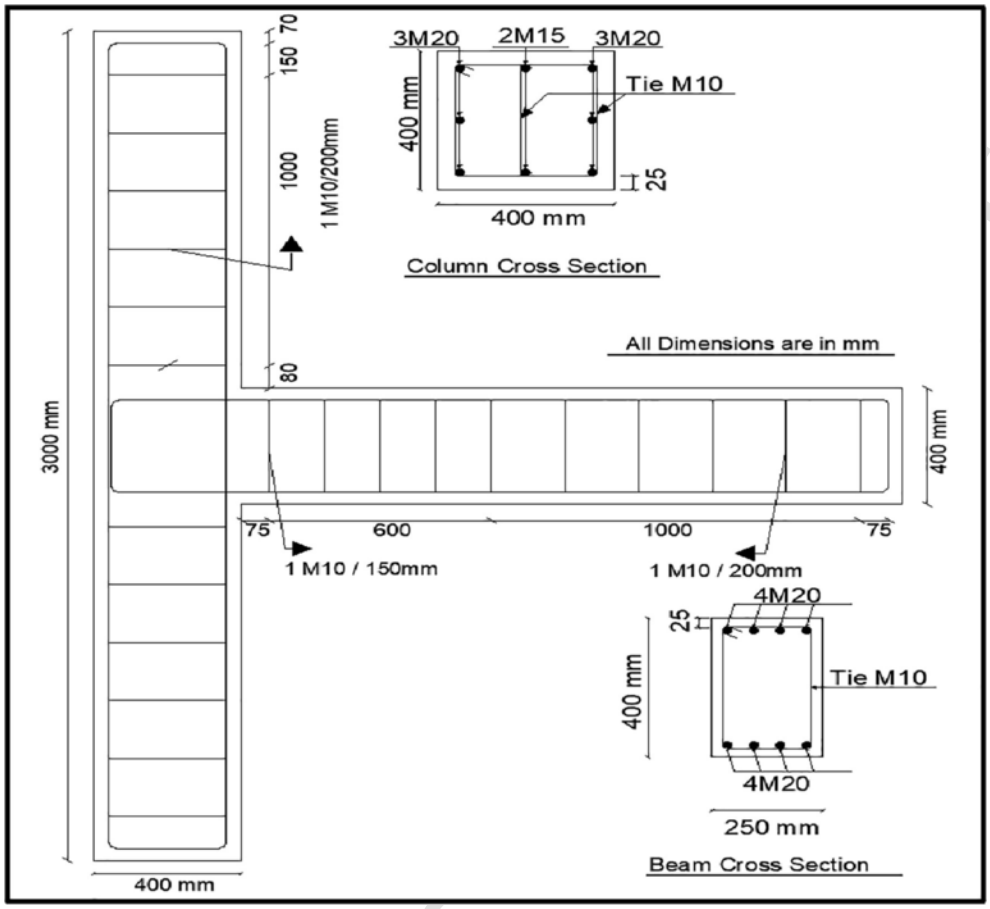


**Fig. 8.** Dimensions and reinforcement details for specimens T-S1, T-S4R and T-S5 [7].

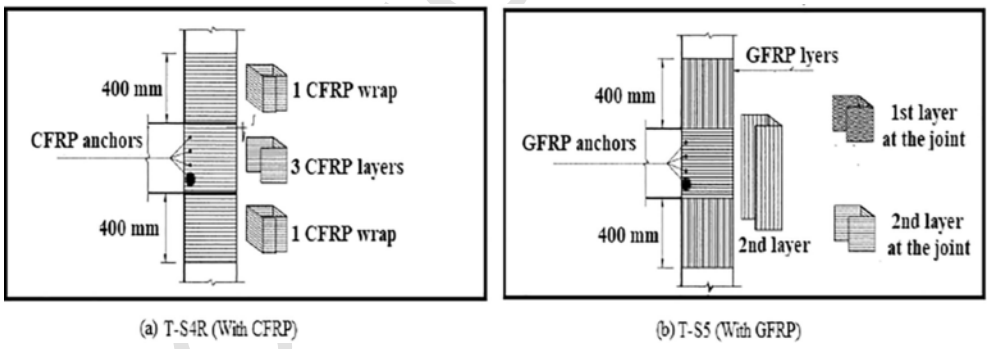


**Fig. 9.** Proposed strengthening techniques for joints T-S4R and T-S5 [7].

creases (or decreases) in all stress directions as plastic straining occurs. Properties of steel for all joints are documented in Table 3.

Bi-linear stress-strain behavior is used for defining the steel for joints Test#2,T-S1, T-S4R and T-S5 with slope hardening equals 0.01Es as assumed by Elmezaini and Ashour [28] in their verification, while full stress-strain diagram which reported by Sharif et al. [26] is used for defining the elasto-plastic behavior steel reinforcement for joints J0, JI0 and JI1because there is no sufficient information about ultimate stress and strain of steel reinforcements from experimental test for these joints. However, the typical stress-plastic strain diagrams for each type of bars are shown in Figs. 12–14. All steels have Young's Modulus (E = 205 GPa) and Poisson's Ratio ($\nu = 0.3$).

*2.4.1.3. Modeling of FRP* Unidirectional FRP sheets are used to strengthen the R.C beam-column joint model. The fiber behavior is linear elastic up to failure with rupture failure. A lamina linear elastic element is used to model FRP as shown in Fig. 15.

The mechanical properties for the combined CFRP sheet and adhesion are evaluated using Eqs. (12)–(17) as proposed by Mallick [29].

$$E_1 = E_f V_f + E_a(1 - V_f) \tag{12}$$

$$E_2 = E_f E_a / (E_a V_f + E_f(1 - V_f)) \tag{13}$$

$$G_{12} = G_{13} = G_f G_a / (G_a V_f + G_f(1 - V_f)) \tag{14}$$

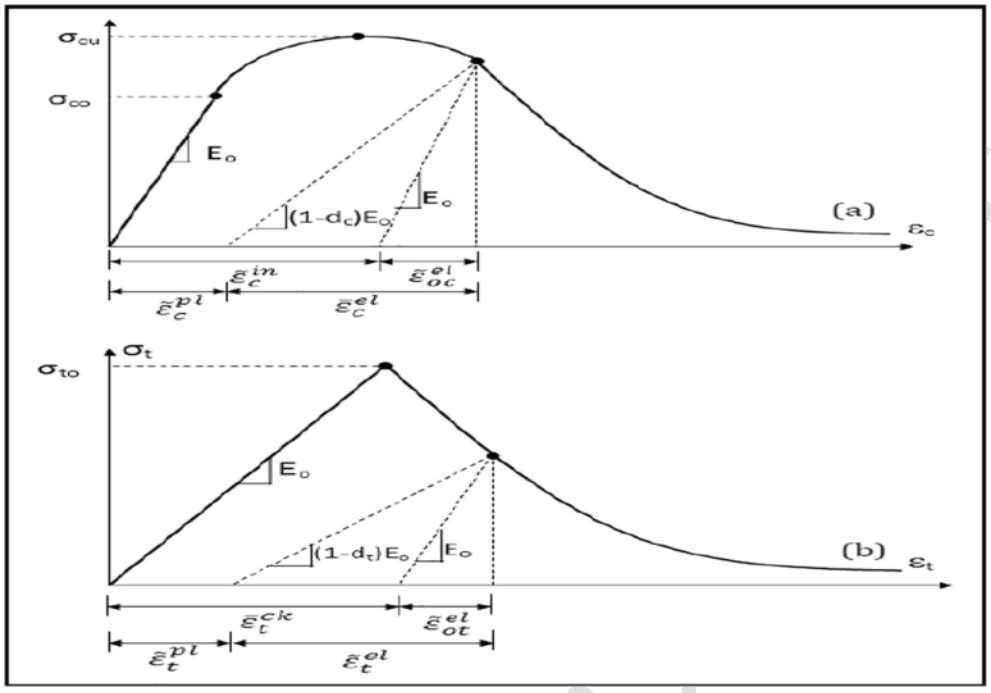


**Fig. 10.** Response of concrete to uniaxial loading in (a) compression and (b) tension [17].

**Table 1**
Parameters of CDP model.

| Parameter name | Value |
|---|---|
| Dilation angle (ψ) | 36° |
| Eccentricity (e) | 0.1 |
| $f_{b0}/f_{c0}$ | 1.16 |
| K | 0.667 |

**Table 2**
Parameters of concrete for joints that used in verification.

| Verification number | Joint ID | Compressive concrete strength (MPa) | $E_0$(MPa) | ν |
|---|---|---|---|---|
| 1 | Test #2 | 46.2 | 30,165 | 0.2 |
| 2,3 and 4 | J0,JI0 and JI1 | 25 | 23,500 | 0.2 |
| 5 | T-S1 | 30.8 | 26,169 | 0.2 |
| 6 | T-S4R | 43.24 | 31,176 | 0.2 |
| 7 | T-S5 | 36.66 | 28,588 | 0.2 |

$$G_{23} = E_2/2(1 + \nu_{23}) \quad (15)$$

$$\nu_{23} = \nu_f V_f + \nu_a(1 - V_f) \quad (16)$$

$$\sigma_{co} = V_f\sigma_u + ((1 - V_f)E_a/E_f)\sigma_u \quad (17)$$

where:

$E_1$: Elastic modulus in the longitudinal direction
$E_2$: Elastic modulus in the transverse direction
$G_{12}$ and $G_{13}$ : Plane shear modulus
$G_{23}$: Normal to the plane shear modulus
ν: Poisson's ratio
$\sigma_{co}$: Ultimate tensile strength
$E_f$: Elastic modulus of CFRP
$V_f$: Volume fraction of CFRP is provided by the manufacturer
$E_a$: Elastic modulus of adhesive material
$G_f$: Shear modulus of CFRP
$G_a$: Shear modulus of adhesive material

The available information about FRP and epoxy for joints strengthened with FRP are summarized in Tables 4 and 5, respectively. Also Table 6 summarizes the properties of combined FRP sheets and adhesive material.

### 2.4.2. Comparisons between F.E and experimental results

Numerical results are compared to experimental data reported by Clyde et al. [11], Mahmoud et al. [8] and El-Amory [7] as shown in Figs. 16–18, respectively. It can be notified that the F.E. model captures the descending branch quite satisfactorily as shown in Figs. 16 and 17. However, Fig. 19a and b show experimental cracks vs. Numerical tensile damage for joints J0 and JI0 at failure stage. This clearly show that the F.E. model is able to predict the experimental cracks accurately.

Based on the above verifications, the F.E. model is able to predict the behavior of exterior R.C beam-column joint strengthened or not strengthened by FRP. This model will be used to investigate the behavior and ductility of exterior R.C beam-column joint. In this research, material is modeled based on parameters on properties documented by Mahmoud et al. [8]. For design purpose, elastic-perfectly plastic steel behavior is used is used in this work with yield strength of 285 MPa for stirrups, while yield strength of longitudinal reinforcement equal 420 MPa as reported by Sharif et al. [26].

### 2.5. Parametric study

Parametric study is conducted to investigate the behavior of exterior R.C beam-column joint strengthened by FRP. The behavior is affected by many parameters. These parameters include: relative inertia

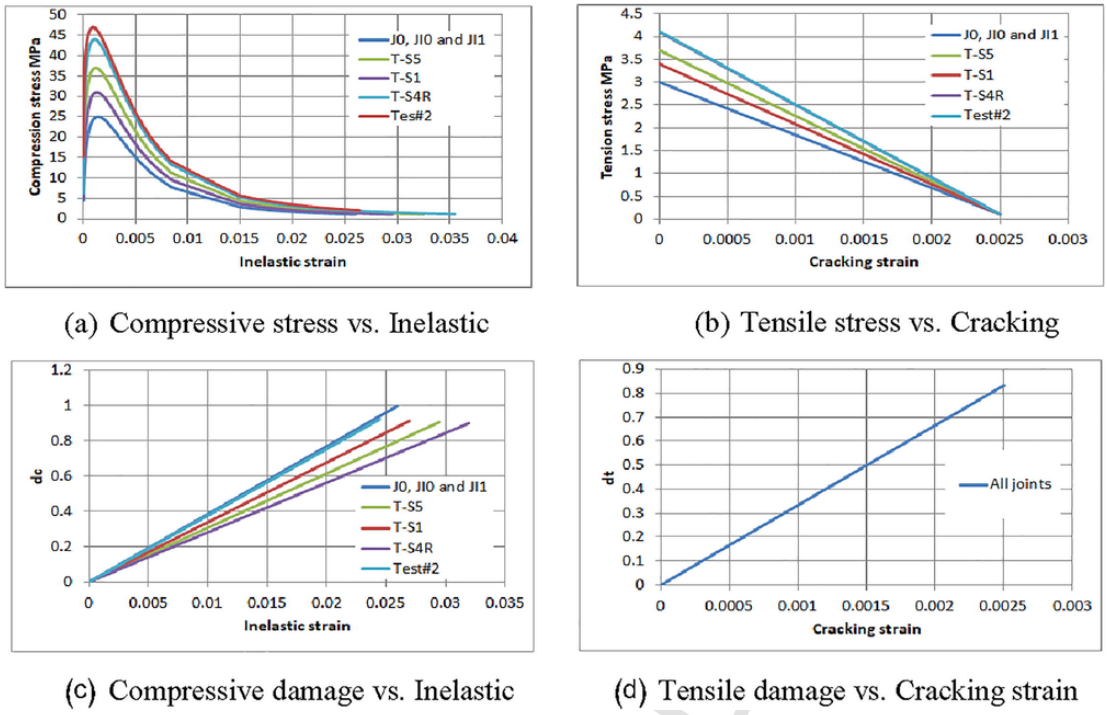


**Fig. 11.** Definition of concrete parameters for CDP model in ABAQUS for joints that used in verification.

**Table 3**
Properties of reinforcement for all joints that used in verification.

| Joint ID | Bar type | Diameter (mm) | Cross sectional area ($mm^2$) | Yield strength (MPa) | Ultimate strength (MPa) |
|---|---|---|---|---|---|
| Test #2 [11] | #9 | 28.65 | 645 | 454.4 | 746 |
| | #7 | 22.225 | 387 | 469.5 | 741.9 |
| | #3 | 9.525 | 71 | 427.5 | 654.3 |
| J0, JI0 and JI1 [8] | ∅16 | 16 | 200.96 | 400 | – |
| | ∅12 | 12 | 113.04 | 400 | – |
| | ∅8 | 8 | 50.24 | 240 | – |
| T-S1, T-S4R and T-S5 [7] | M10 | 11.3 | 100.29 | 477 | 720 |
| | M15 | 16 | 201.06 | 409.5 | 617.5 |
| | M20 | 19.5 | 298.65 | 477 | 764 |

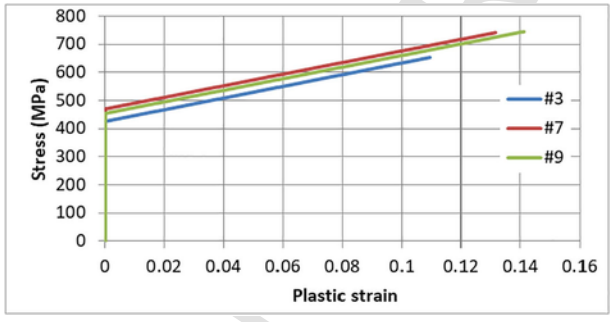


**Fig. 12.** Stress –plastic strain diagrams for steel, joint (Test#2).

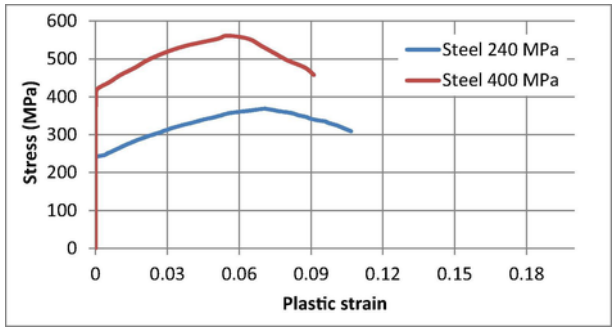


**Fig. 13.** Stress –plastic strain diagrams for steel 240 MPa and 400 MPa, joints (J0, JI0 and JI1).

between column and beam (G), amount of transverse steel in joint $(Av/s)_J$, amount of transverse steel in beam $(Av/s)_B$, longitudinal steel ratio (ρ), axial load on column (N), number of CFRP layers (n) and shear to moment ratio. Four main parameters are investigated in this research. Those parameters have clear influence on the behavior as reported by many researchers, which are relative inertia of column relative to beam (G), shear reinforcement in joint $(Av/s)_J$, shear reinforcement in beam $(Av/s)_B$ and the effect of CFRP. At the same time, other variables (such as axial force, longitudinal steel ratio, number of CFRP layers and shear to moment ratio) are kept constant for the seek of the selected parameters. The mentioned variables are investigated numerically as ductility point of view.

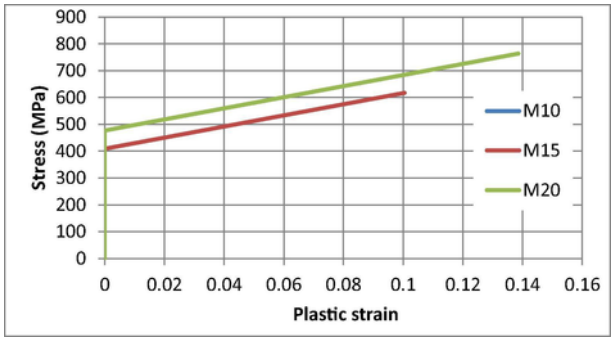


**Fig. 14.** Stress –plastic strain diagram for steel, joints (T-S1, T-S4R and T-S5).

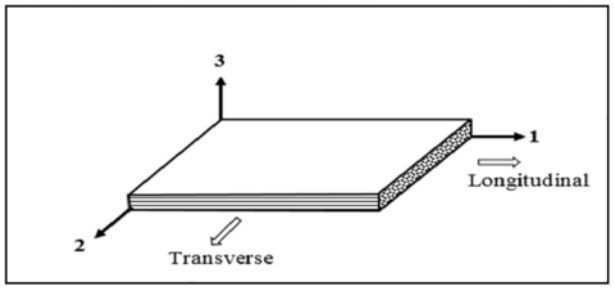


**Fig. 15.** Schematic of unidirectional FRP lamina.

A total of 48 simulations have been conducted on R.C joints with and without CFRP. The layout of the CFRP is assumed as wraps around beam member only with one layer of CFRP sheet for all models as shown in Fig. 20. This schematic arrangement is selected as one of the effective strengthening techniques as stated by many researchers [30–32]. To simulate the service axial load in real structure, a compression force of 1050 kN is applied on column (0.26 Ag $f'c$) where, Ag is the gross sectional area of column and $f'c$ is the compressive strength of concrete.

## 3. Results and discussion

Four main parameters are investigated in this section, these includes: relative inertia (G) having three different levels starting by 0.512 that presents strong beam- weak column, up to 4.63 presenting weak beam-strong column and an intermediate case with ratio equals to 1.0. Second parameter is shear reinforcement in beam $(Av/s)_B$ having four different levels starting by 0.5 $mm^2$/mm that presents minimum value up to maximum value which equals 4.5 $mm^2$/mm and two intermediate cases with values 1.13 an 3.14 $mm^2$/mm. Third parameter is Shear reinforcement in joint $(Av/s)_J$ having two values which equal 0.5 and 4.5 $mm^2$/mm. In addition, effect of wrapping CFRP is investigated beside the above three parameters.

### 3.1. Effect of joint stirrups continuity $(Av/s)_J$

The resulting curves for cases without CFRP are shown in Figs. 21–23 which present the effect of joint stirrups continuity for models with relative inertia (G) equals 0.512, 1 and 4.63, respectively. Results show that, stirrups continuity inside the joint increases the capacity remarkably for models with G equals 0.512 which are dominated by shear failure of joint or beam. However, small effect of stirrups continuity inside the joint for G equals 1, while there is no effect of stirrups continuity inside the joint for G equals 4.63, since the flexural capacity of the beam is less than shear capacity of joint. In addition, ductility decreases when using minimum shear reinforcement in beam and maximum shear reinforcement in the joint. This is logical because the load-deflection curve becomes stiffer due to strengthening of joint, therefore sudden failure happens in the beam due to shear. The same behavior is observed for CFRP models, but the ductility remains approximately constant for all models with CFRP because no shear failure happens in beam. This is shown in Figs. 24–26 which present the effect of joints stirrups continuity for models with relative inertia (G) equals 0.512, 1 and 4.63, respectively.

### 3.2. Effect of relative inertia (G)

The resulting curves for cases without CFRP are shown in Figs. 27 and 28 which present the effect of relative inertia for models with $(Av/s)_J$ equals 4.5 and 0.5, respectively. Results show that, generally, as relative inertia decreases, the ultimate capacity increases and the ductility decrease. This is logical because decreasing G means larger beam. This trend is also exists for the case of using CFRP as shown in Figs. 29 and 30 which present the effect of relative inertia for models with $(Av/s)_J$ equals 4.5 and 0.5, respectively. However, by using CFRP, the shear failure which is predicted to happen in beam converts to flexure failure in beam or shear failure in joint depending on the amount of stirrups continuity inside the joint.

### 3.3. Effect of beam stirrups $(Av/s)_B$

Load-deflection curves for beam-column joints strengthened by CFRP are shown in Figs. 31 and 32. Different joints with different spacing between beam stirrups are simulated using two values of $(Av/s)_J$ which equal 4.5 and 0.5 $mm^2$/mm. Generally, it can be seen that for small values of $(Av/s)_B$ in cases of maximum $(Av/s)_J$, the failure is dominated by shear in beam and therefore it is a brittle failure. As the value of $(Av/s)_B$ increases, the ductility increases mainly due to shear strengthening. On the other hand, in cases of minimum $(Av/s)_J$, as the value of $(Av/s)_B$ increases, the failure becomes shear failure in the joint. This is due to strong beam-weak joint for this case.

The results show that the ductility increases with increasing the transverse steel up to a certain value of $(Av/s)_B$ that mainly depends on relative inertia and joint stirrups. Those values defined as $(Av/s)^o_B$ and summarized in Table 7. Increasing $(Av/s)_B$ beyond this value has no significant effect on ductility. This trend does not happen when using CFRP, because using CFRP converts brittle failure to ductile failure as shown in Figs. 33 and 34, which present the effect of beams stirrups for models with $(Av/s)_J$ equals 4.5 and 0.5, respectively.

### 3.4. Effect of using CFRP

Generally, CFRP is used to strengthen the joints and prevent brittle failure. The curves for the cases with maximum and minimum $(Av/s)_J$

**Table 4**
Properties of FRP sheets for joints JI1, T-S4R and T-S5.

| Joint ID | Fiber type | Ultimate tensile strength (MPa) | Ultimate strain (%) | Modulus of elasticity (MPa) | Thickness (mm) |
|---|---|---|---|---|---|
| JI1 | CFRP | 3500 | 1.5 | 230,000 | 0.13 |
| T-S4R | CFRP | 3550 | 1.5 | 235,000 | 0.165 |
| T-S5 | GFRP | 575 | 2.2 | 26,100 | 1.3 |

**Table 5**
Properties of epoxy for installing FRP sheets for joints JI1, T-S4R and T-S5.

| Joint ID | Epoxy type | Tensile strength (MPa) | Tensile modulus (MPa) | Ultimate elongation (%) |
|---|---|---|---|---|
| JI1 | Epoxy for installing CFRP | 30 | 21,400 | 4.8 |
| T-S4R | Epoxy for installing CFRP | 14 | 1138 | 5.3 |
| T-S5 | Epoxy for installing GFRP | 72.4 | 3180 | 5 |

are shown in Figs. 35 and 36, respectively. Results show that, generally, using CFRP converts the brittle failure to a ductile failure. However, there is no significant effect of using CFRP when models reach maximum confinement due to beam stirrups or when failure happens inside the joint. On the other hand, the effect of CFRP is remarkable for models that are dominated by shear failure of beam. For instance, Fig. 37 shows the cracks at failure stages before and after wrapping CFRP for joint with relative of inertia (G) equals 0.512, maximum stirrups inside joint ($(Av/s)_J = 4.5$) and minimum stirrups inside beam ($(Av/s)_B = 0.5$).

## 4. Conclusions

In this paper, three-dimensional (3-D) non-linear finite element (F.E.) model of an exterior R.C beam-column joint is verified and then used to study the ductility of beam-column joint. Different parameters are investigated and discussed in this study. Based on this study, the following conclusions are summarized:

- The behavior of the joint is complex and critical for overall structural behavior. Brittle behavior must be avoided so that a ductile failure mode should be the dominator.
- The developed F.E. model produced realistic and accurate results, and captured the nonlinear complex behavior of the joint. The model included most types of nonlinearities, including plasticity damage in concrete and nonlinear contact behavior and geometric nonlinearities.
- Using CFRP wraps around beam converts the brittle failure to ductile failure. However, there is no effect of CFRP when models reach maximum confinement due to beam stirrups or when failure happens inside the joint. On the other hand, the effect of CFRP wrapping is significant for models that are dominated by only shear failure of beam.
- CFRP strengthening approach for beam-column joints extremely effected by initial design. Poor design could be strengthened efficiently for both; carrying capacity and ductility using CFRP.
- Results show that, stirrups continuity inside the joint increases the capacity and ductility for models dominated by shear failure. This behavior also happens for models with CFRP, but with small increase in ductility.
- As relative stiffness ratio decreases, the ultimate capacity increase and the ductility decrease. This is logical because decreasing of G means larger beam. This trend also exists for the case of using CFRP.
- Ductility increases with increasing the transverse steel up to a certain maximum value of $(Av/s)_B$ which can be called a fixed value. Increasing $(Av/s)_B$ beyond this maximum value causes no significant effect on ductility. This value depends on the relative inertia (G) and amount of stirrups inside the joint $(Av/s)_J$. This trend does not happen when using CFRP, because using CFRP converts brittle failure to ductile failure.

## Acknowledgement

The authors wish to thank Dr. Mohammad Abu-Jafar for the technical support and the use of mainframe workstations for carrying out the numerical simulations.

**Table 6**
Properties for combined FRP sheets with matrix for joints JI1, T-S4R and T-S5.

| Joint ID | Type of FRP | E1 (MPa) | E2 (MP) | $\nu 12$ | G12 (MPa) | G13 (MPa) | G23 (MPa) | Knn (N/mm3) | Kss (N/mm3) | Ktt (N/mm3) |
|---|---|---|---|---|---|---|---|---|---|---|
| JI1 | CFRP | 106,509 | 33,970 | 0.31 | 12,400 | 12,400 | 13,065 | 1300 | 1300 | 1300 |
| T-S4R | CFRP | 96,554 | 1916 | 0.31 | 750 | 750 | 750 | 515 | 515 | 515 |
| T-S5 | GFRP | 12,531 | 4955 | 0.31 | 1800 | 1800 | 1800 | 600 | 600 | 600 |

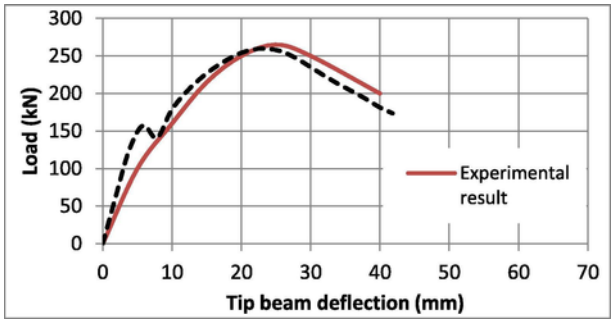


**Fig. 16.** Comparison between experimental and F.E. results for specimen (Test#2) which tested by Clyde et al. [11].

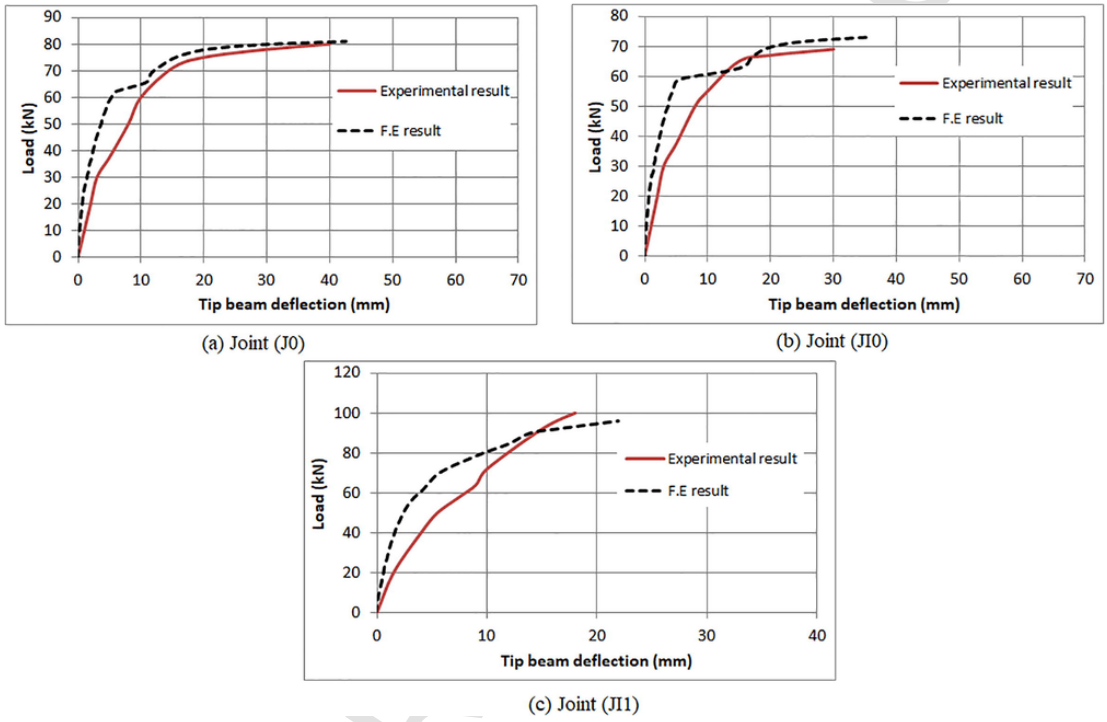


**Fig. 17.** Comparison between experimental and F.E. results for joints J0, JI0 and JI1 tested by Mahmoud et al. [8].

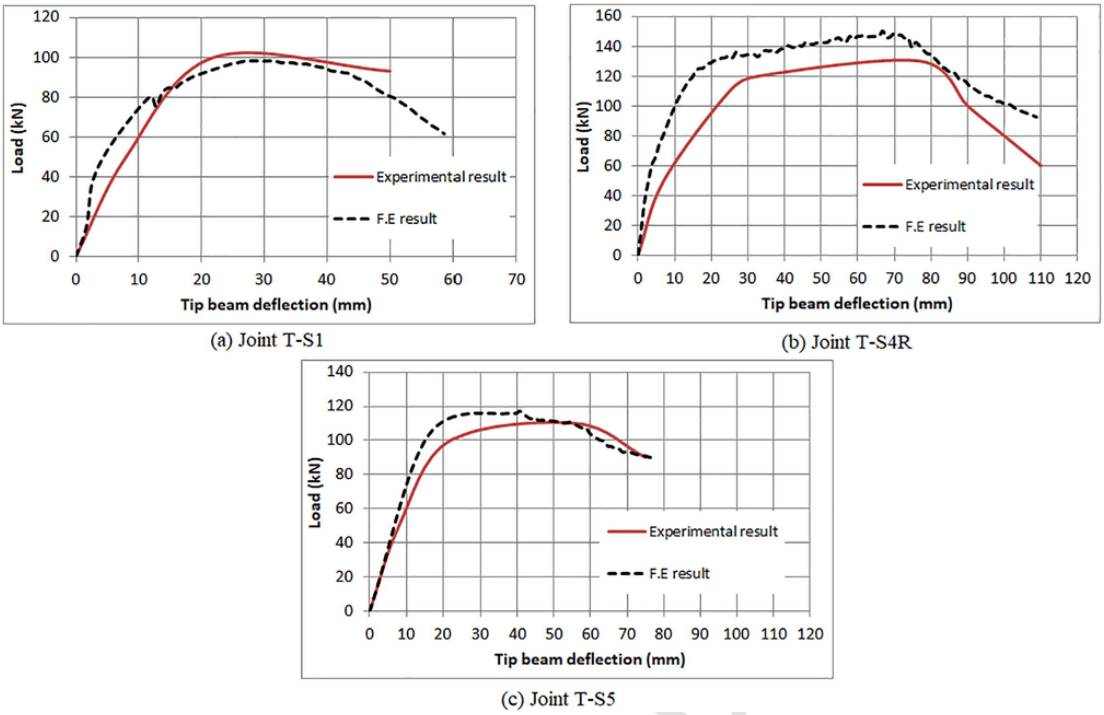


**Fig. 18.** Comparison between experimental and F.E. results for joints T-S1, T-S4R and T-S5 tested by El-Amoury [7].

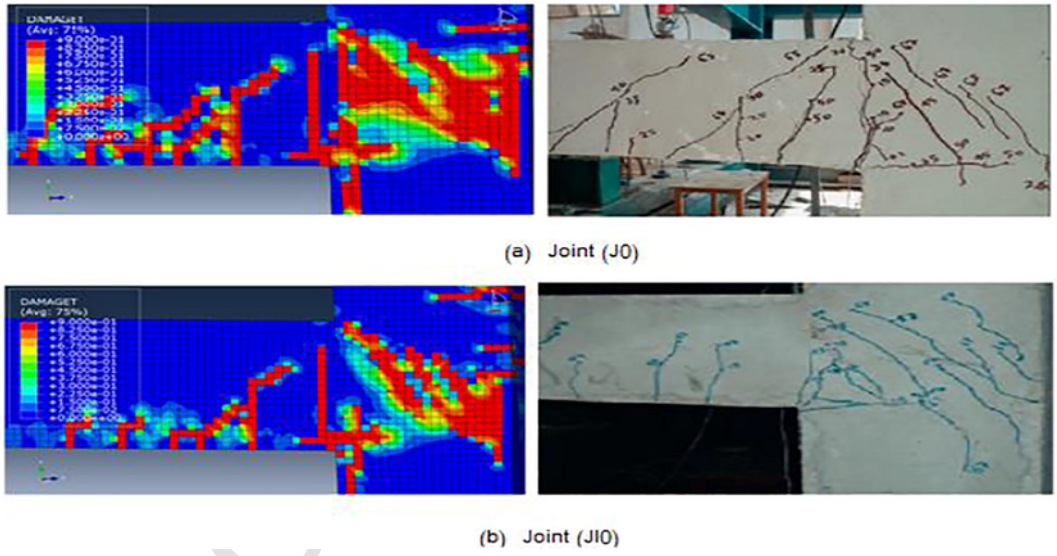


**Fig. 19.** Comparison between tension damage from F.E and experimental test for joints J0 and JI0 tested by Mahmoud et al. [8].

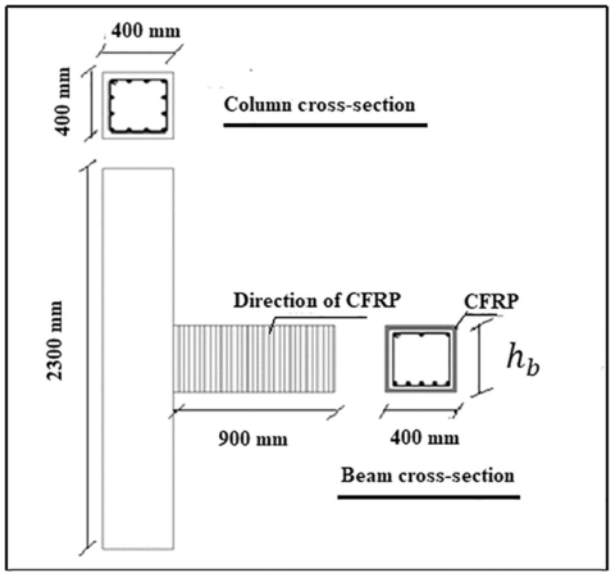


**Fig. 20.** Typical wrapping arrangement of CFRP.

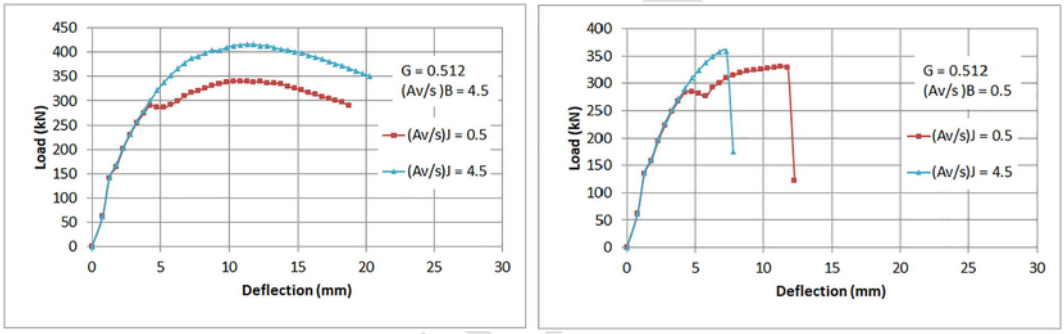


**Fig. 21.** Effect of joints stirrups continuity on strength and ductility of joints with G equals 0.512 without CFRP.

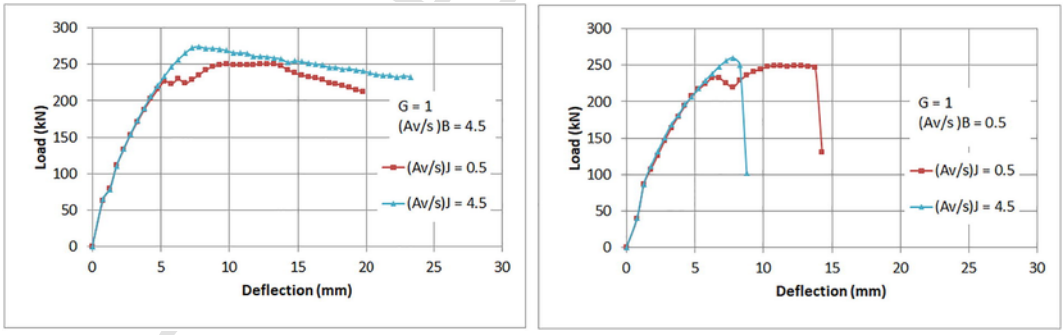


**Fig. 22.** Effect of joints stirrups continuity on strength and ductility of joints with G equals 1 without CFRP.

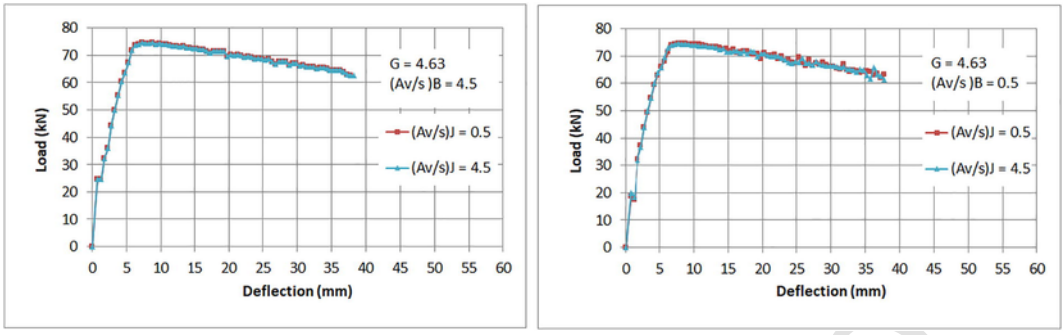


**Fig. 23.** Effect of joints stirrups continuity on strength and ductility of joints with G equals 4.63 without CFRP.

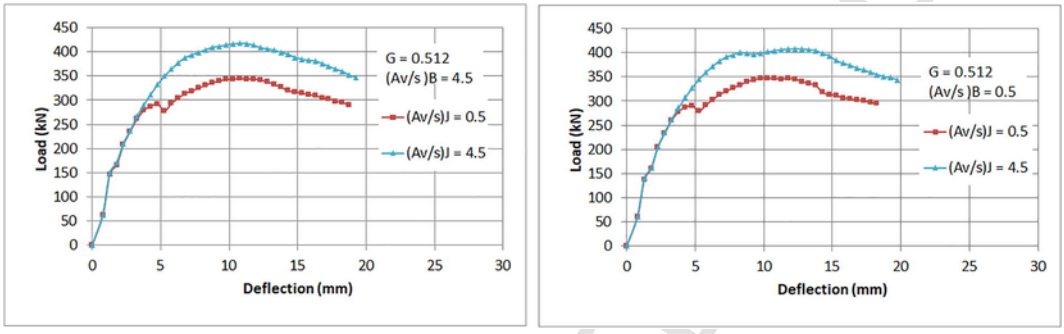


**Fig. 24.** Effect of joints stirrups continuity on strength and ductility of joints with G equals 0.512 strengthened with CFRP.

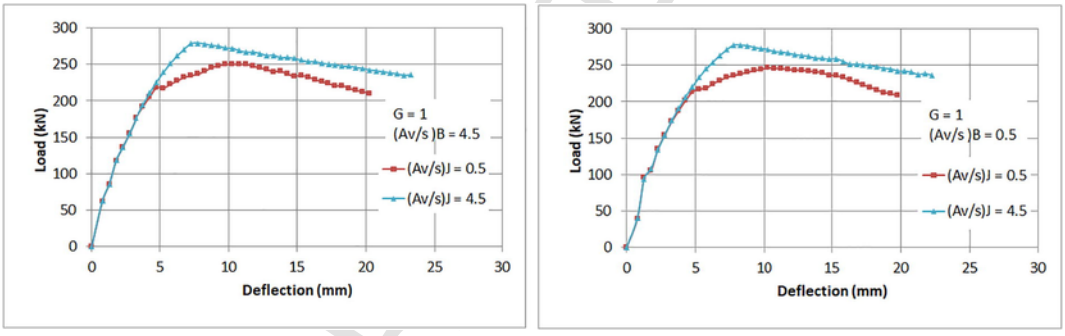


**Fig. 25.** Effect of joints stirrups continuity on strength and ductility of joints with G equals 1 strengthened with CFRP.

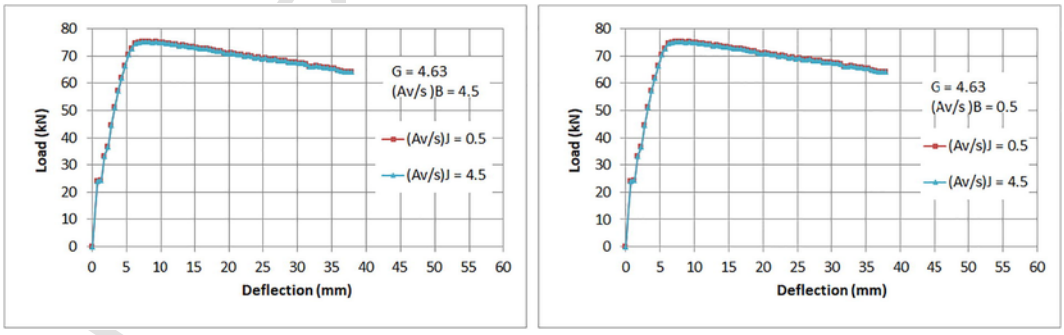


**Fig. 26.** Effect of joints stirrups continuity on strength and ductility of joints with G equals 4.63 strengthened with CFRP.

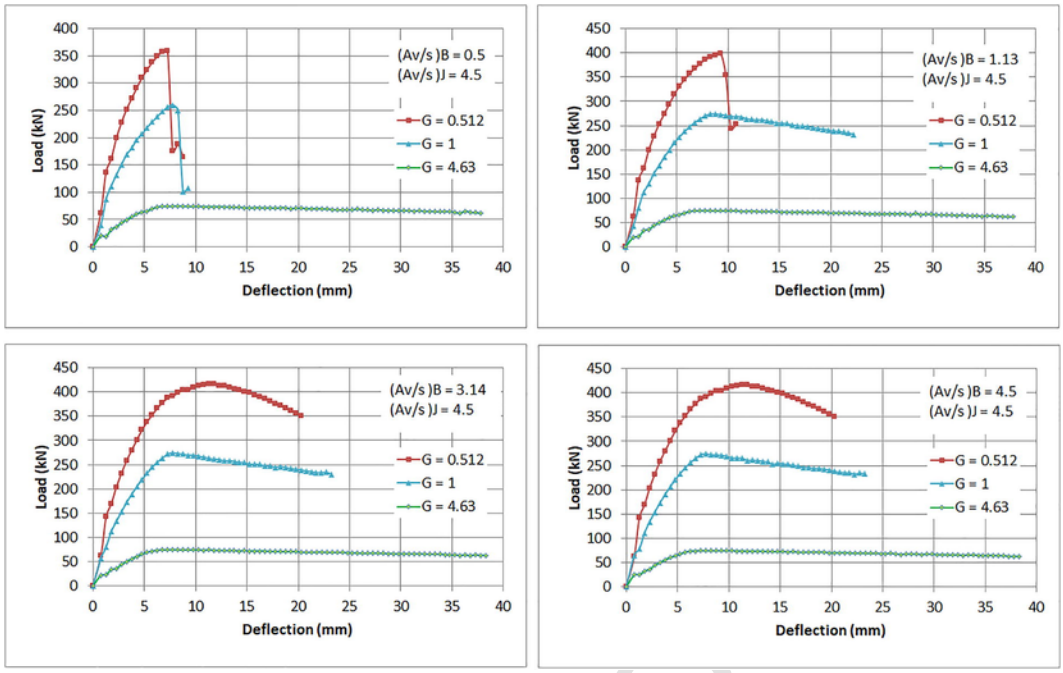


**Fig. 27.** Effect of relative inertia on strength and ductility of joints with maximum $(Av/s)_J$ without CFRP.

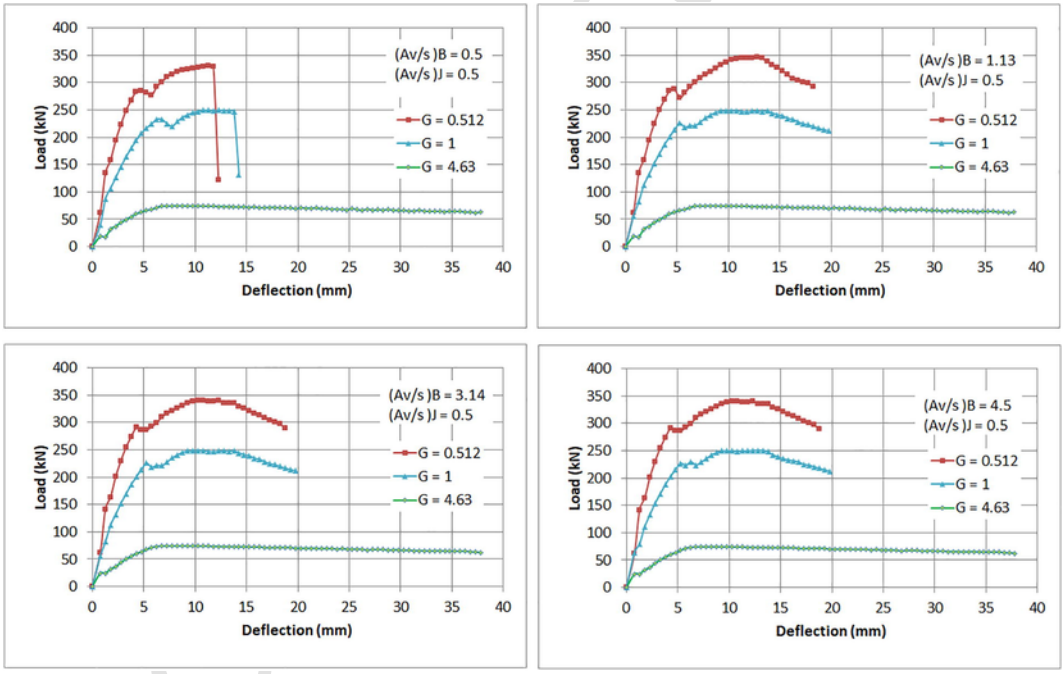


**Fig. 28.** Effect of relative inertia on strength and ductility of joints with minimum $(Av/s)_J$ without CFRP.

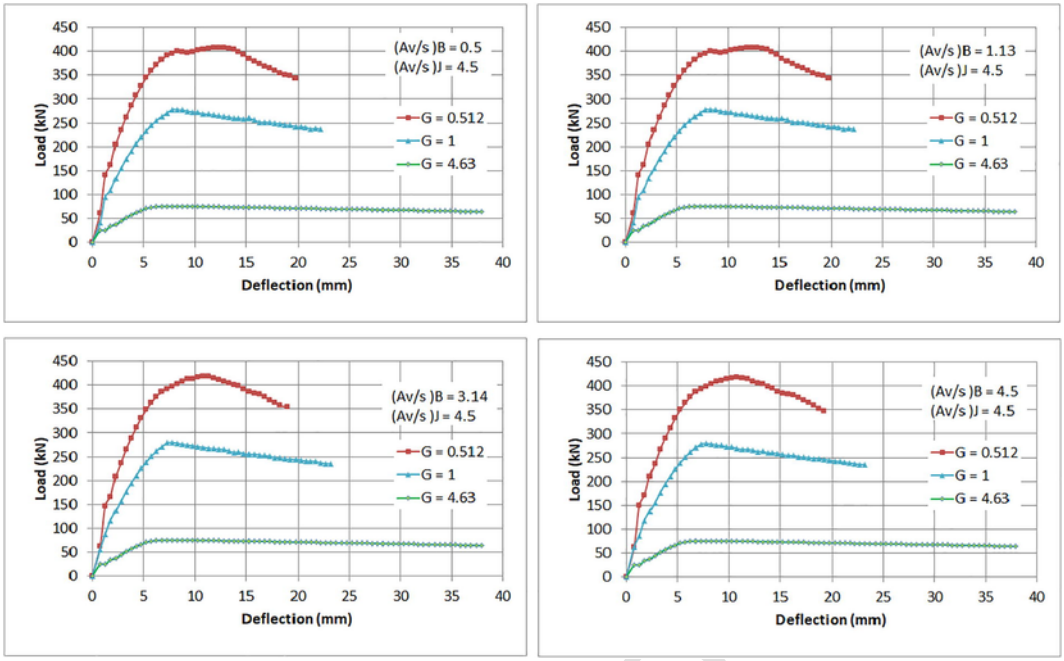


**Fig. 29.** Effect of relative inertia on strength and ductility of joints with maximum $(Av/s)_J$ strengthened with CFRP.

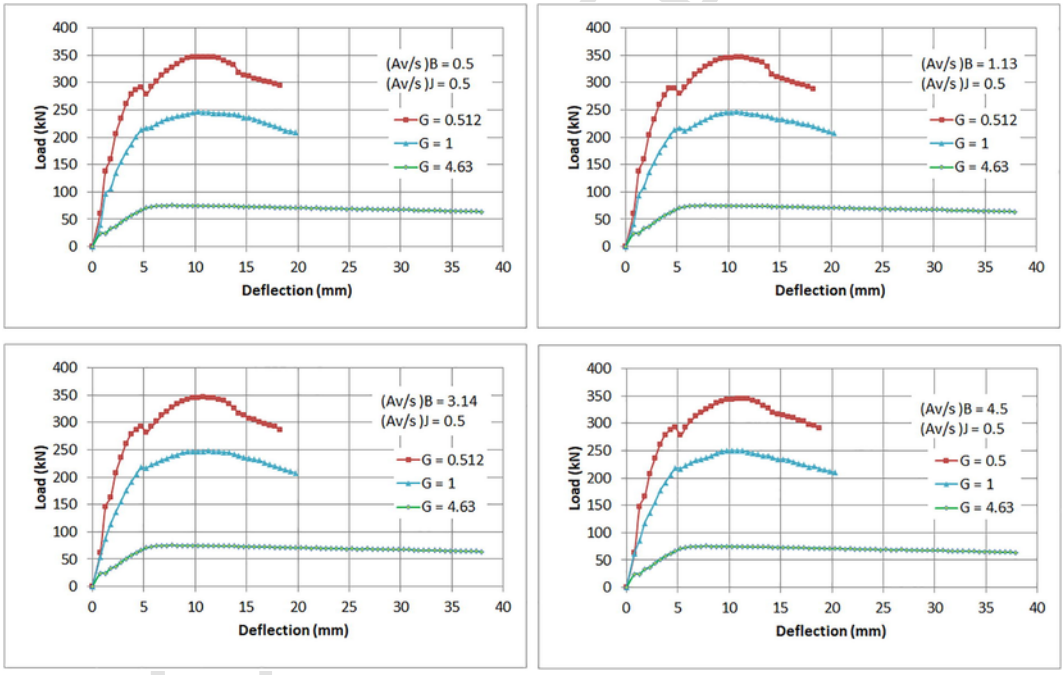


**Fig. 30.** Effect of relative inertia on strength and ductility of joints with minimum $(Av/s)_J$ strengthened with CFRP.

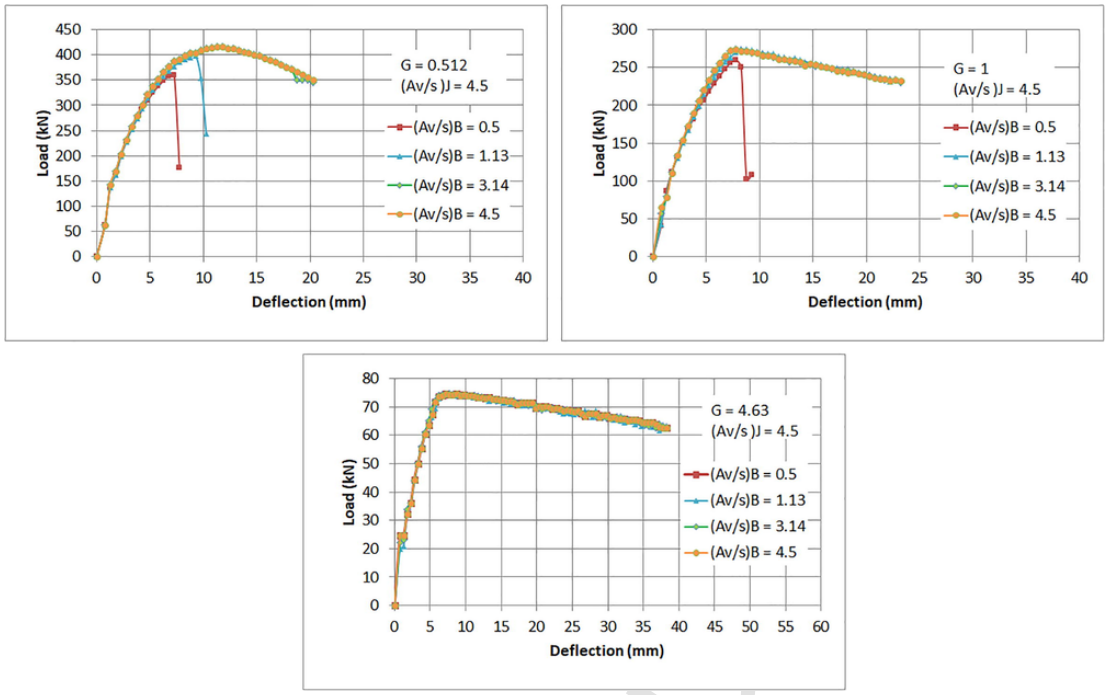


**Fig. 31.** Effect of beams stirrups on strength and ductility of joints with maximum $(Av/s)_J$ without CFRP.

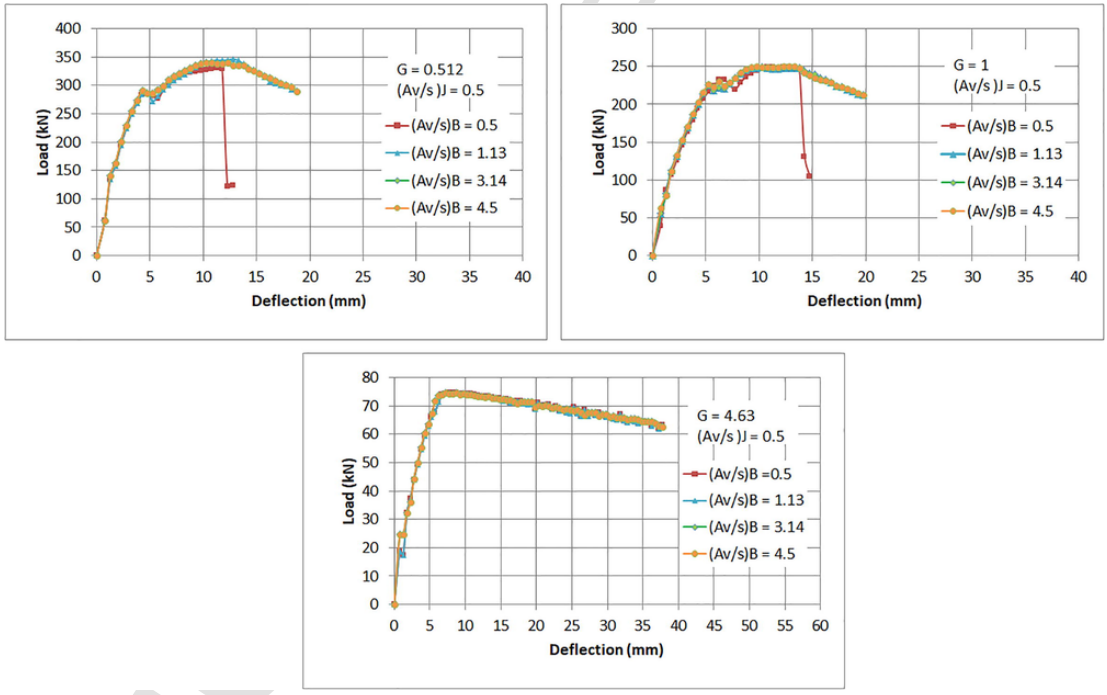


**Fig. 32.** Effect of beams stirrups on strength and ductility of joints with minimum $(Av/s)_J$ without CFRP.

**Table 7**
Maximum value of $(Av/s)^o_B$ beyond which it has no effect on ductility.

| G | $(Av/s)_J$ ($mm^2/mm$) | $(Av/s)^o_B$ ($mm^2/mm$) |
|---|---|---|
| 0.512 | 0.5 | 1.13 |
| | 4.5 | 3.14 |
| 1 | 0.5 | 1.13 |
| | 4.5 | 1.13 |
| 4.63 | 0.5 | 0.5 |
| | 4.5 | 0.5 |

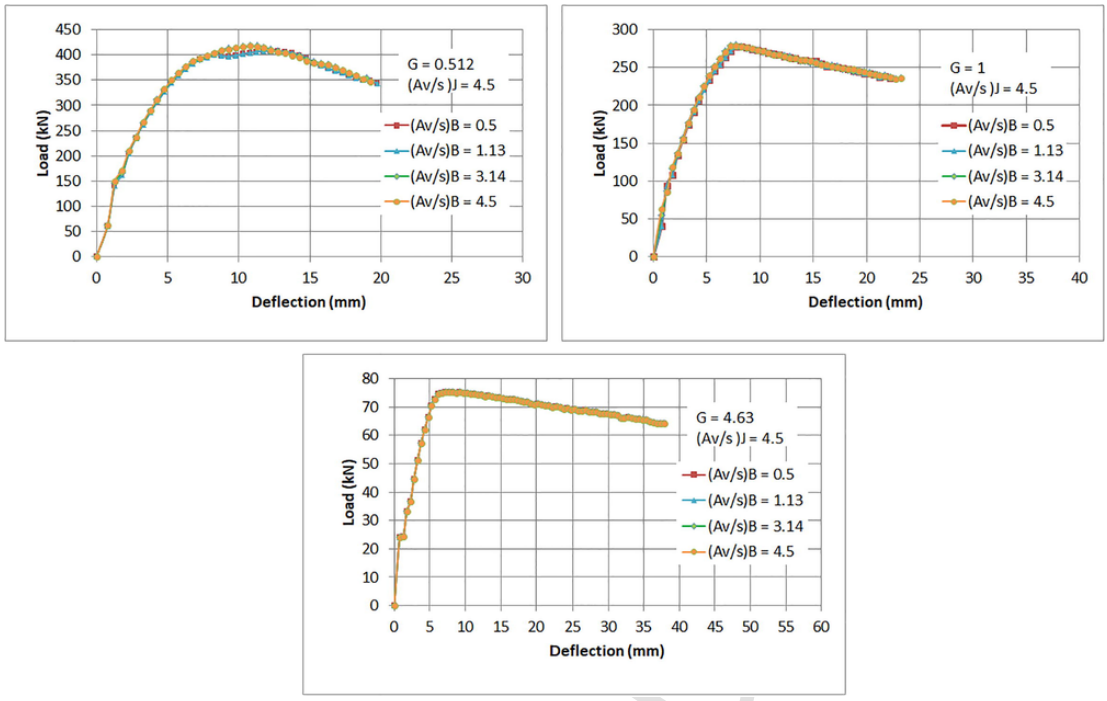


**Fig. 33.** Effect of beams stirrups on strength and ductility of joints with maximum $(Av/s)_J$ strengthened with CFRP.

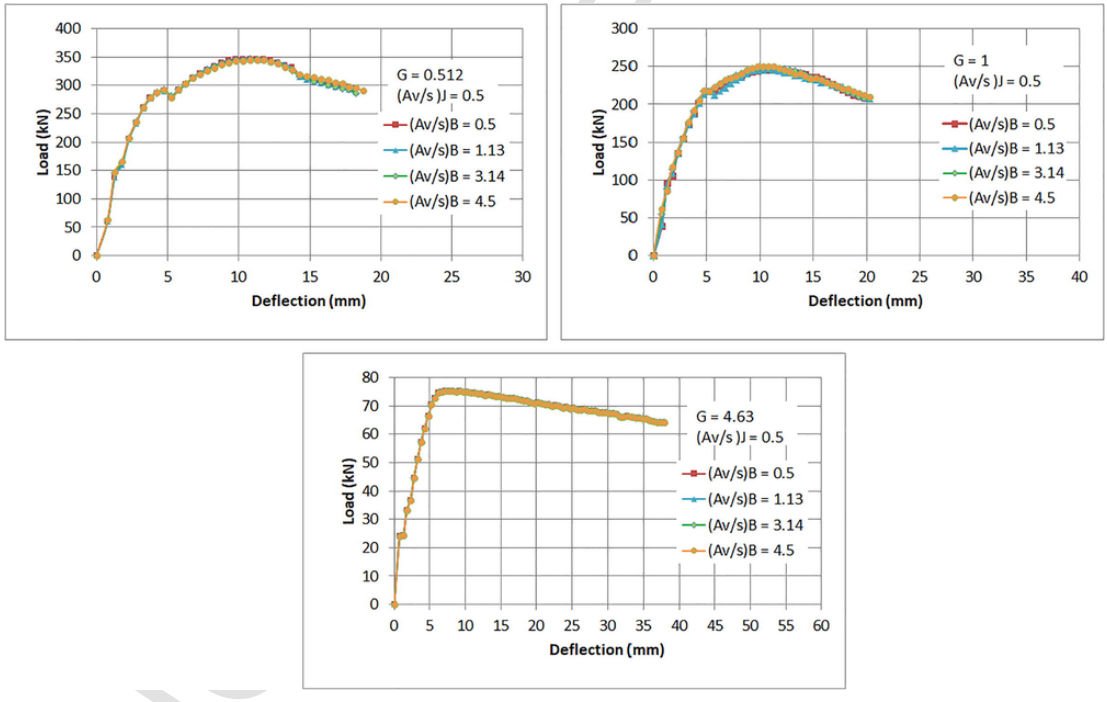


**Fig. 34.** Effect of beams stirrups on strength and ductility of joints with minimum $(Av/s)_J$ strengthened with CFRP.

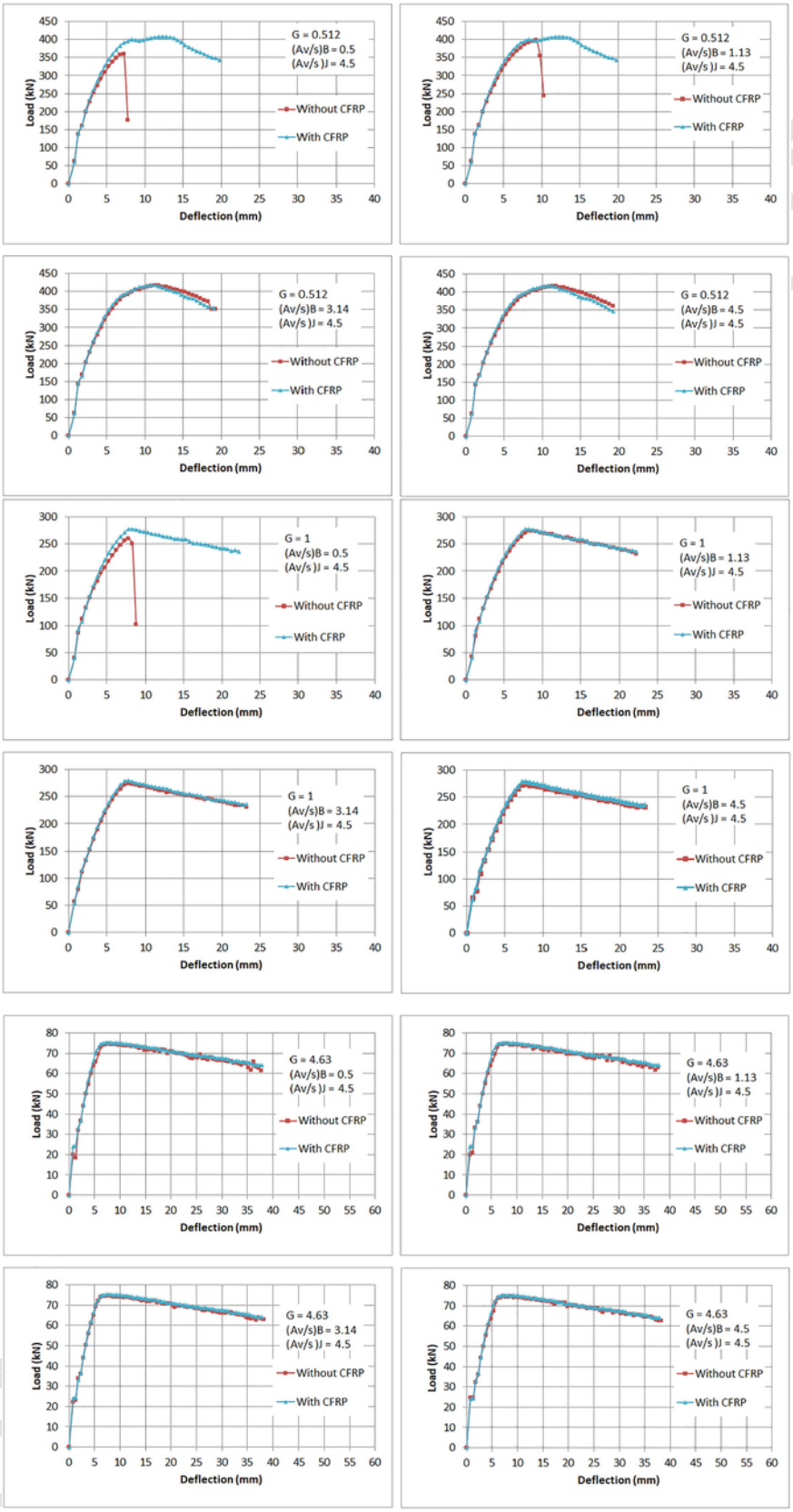


**Fig. 35.** Effect of CFRP on strength and ductility of joints with maximum $(Av/s)_J$.

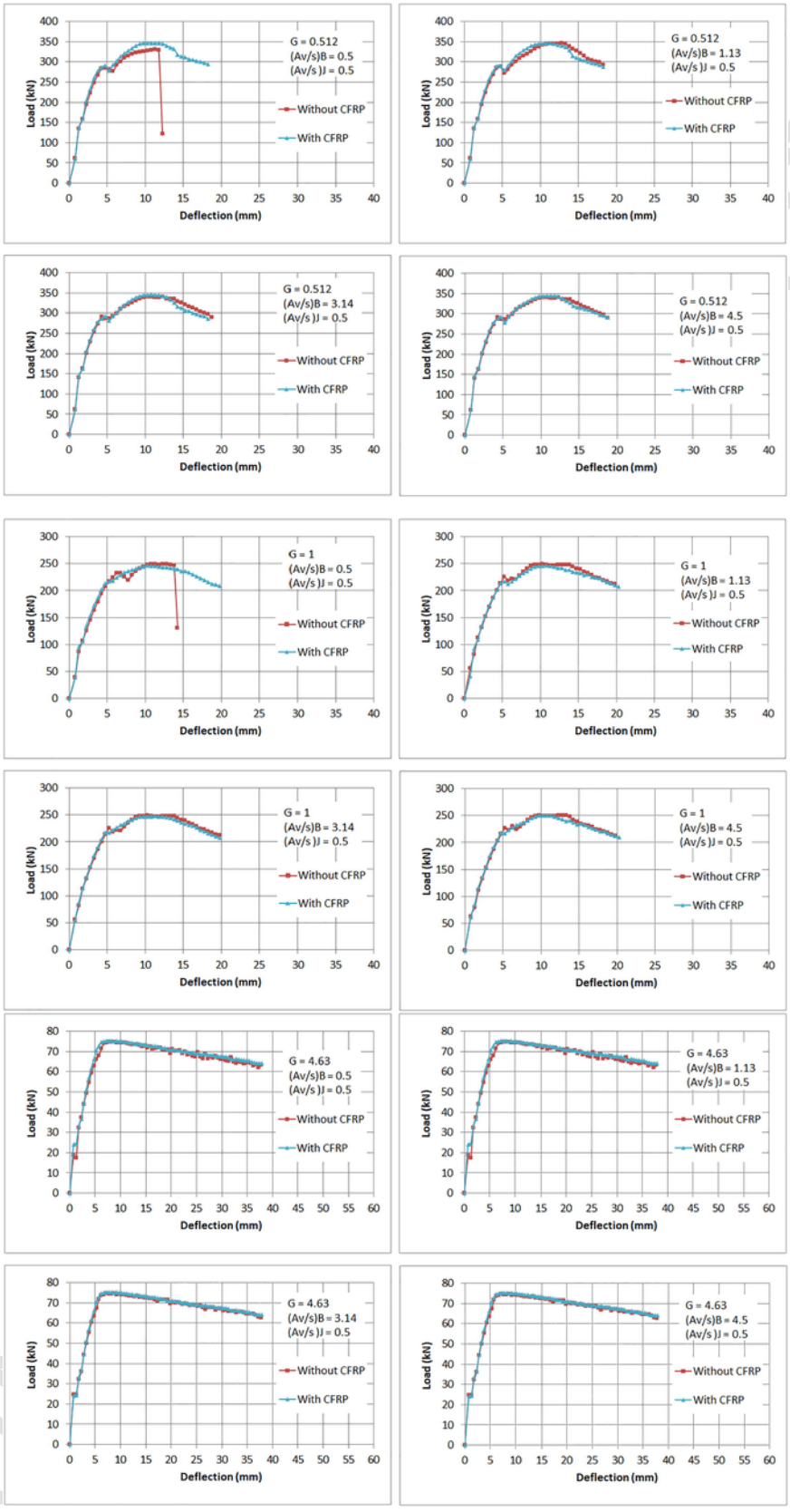


**Fig. 36.** Effect of CFRP on strength and ductility of joints with minimum $(Av/s)_J$.

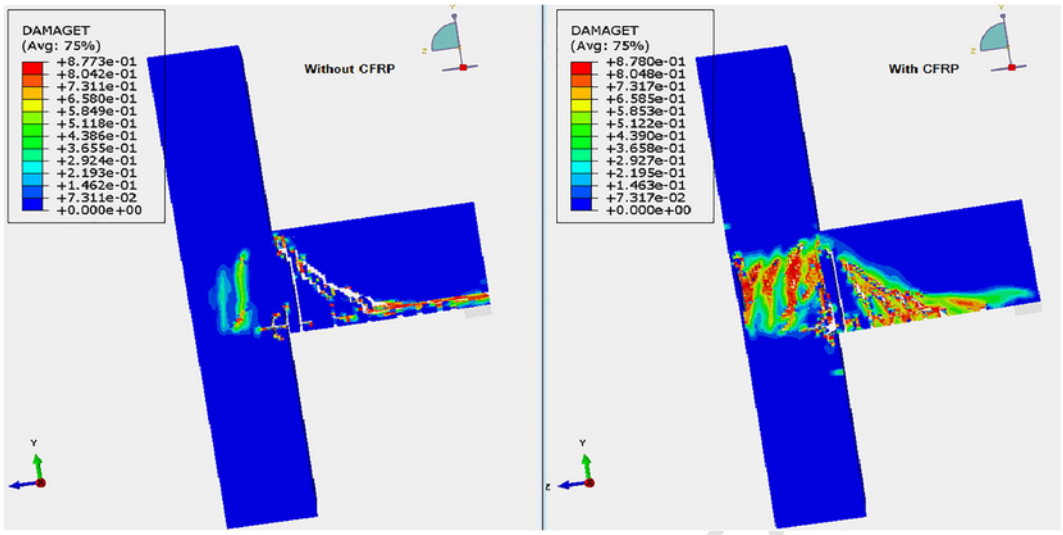


**Fig. 37.** Cracks at failure before wrapping CFRP for joint with G = 0.512, $(Av/s)_J = 4.5$ and $(Av/s)_B = 0.5$.

## References


[1] K.R. Siva Chidambaram, G.S. Thirugnanam, Comparative studies on behavior of reinforced beam-column joints with reference to anchorage detailing, J Civ Eng Res 2 (4) (2013) 12–17.

[2] A.K. Kaliluthin, S. Kothandaraman, T.S. Suhail-Ahamed, A review on behavior of reinforced concrete beam-column joint, Int J Innovative Res Sci Eng Technol 3 (4) (2014) 11299–11312.

[3] S.R. Uma, A.M. Prasad, Seismic behavior of beam column joints in reinforced concrete moment resisting frames. Department of civil engineering, Indian Institute of technology Madras, Chennai, Document, 19961.

[4] A. Ghobarah, T.S. Aziz, A. Biddah, Seismic rehabilitation of reinforced concrete beam-column connections, J Earthquake Spectra 12 (4) (1996) 761–780.

[5] Jing LI, Pam HJ, Francis TK. New details of HSC beam-column joints for regions of low to moderate seismicity. In 13th World conference on earthquake engineering, Vancouver, Canada; 2004. (449).

[6] A. Ghobarah, A. Said, Seismic rehabilitation of beam-column joints using frp laminates, J Earthquake Eng 5 (1) (2001) 113–129.

[7] A.T. El-Amoury, Seismic rehabilitation of concrete frame beam-column joints, [Ph.D. Thesis] McMaster University, Ontario, Canada, 2004.

[8] M.H. Mahmoud, H.M. Afefy, N.M. Kassem, T.M. Fawzy, Strengthening of defected beam-column joints using CFRP, J Adv Res 5 (1) (2014) 67–77.

[9] M.A. Samaaneh, A.M. Sharif, M.H. Baluch, A.K. Azad, Numerical Investigation of continuous composite girders strengthened with CFRP, J Steel Compos Struct 21 (6) (2016) 1307–1325.

[10] S.T. Bidgar, P. Bhattacharya, Nonlinear finite element analysis of reinforced concrete exterior beam column joint subjected to monotonic loading, RTCET STM J 4 (2) (2014) 1–10.

[11] Clyde C, Pantelides CP, Reaveley RD. Performance based evaluation of exterior reinforced concrete building joints for seismic excitation. PEER Report 2000/05 Pacific Earthquake Research Center, College of Engineering University of California, Berkeley; 2000.

[12] ABAQUS version 6.13). [Computer software]. Assault Systems. Waltham. MA; 2013.

[13] Y.B. Abu-Tahnat, Effect of using fiber reinforced polymers on the ductility of retrofitted reinforced concrete joint, [MSc. Thesis] An-Najah National University, Nablus, Palestine, 2018.

[14] S.V. Chaudhari, K.A. Mukane, M.A. Chakrabarti, Comparative study on exterior RCC beam column joint subjected to monotonic loading, Int J Comput Appl 102 (3) (2014) 34–39.

[15] Neubauer U, Rostasy FS. Bond failure of concrete fiber reinforced polymer plates at inclined Cracks—experiments and fracture mechanics model. In: Proc., 4th Int. symp. on fiber-reinforced polymer reinforcement for reinforced concrete structures, SP-188, American Concrete Institute, Farmington Hills, Mich. 1999; 369–382.

[16] Obaidat YT, Heyden S, Dahlblom O. Bond action between frp and concrete–a new model. Structural retrofitting of concrete beams using FRP; 2011.

[17] ABAQUS: ABAQUS Analysis User's Manual Version 6.13. Assault Systems; 2013.

[18] Wahalathantri BL, Thambiratnam DP, Chan THT, Fawzia S. Material model for flexural crack simulation in reinforced concrete elements using ABAQUS. In: Proceedings of the first international conference on engineering, designing and developing the built environment for sustainable wellbeing; 2011: 260–264.

[19] J. Lubliner, J. Oliver, S. Oller, E. Onate, A plastic-damage model for concrete, Int J Solids Struct 25 (3) (1989) 299–326.

[20] J. Lee, G.L. Fenves, Plastic-damage model for cyclic loading of concrete structures, J Eng Mech 124 (8) (1998) 892–900.

[21] J.B. Mander, M.J. Priestley, R. Park, Theoretical stress-strain model for confined concrete, J Struct Eng 114 (8) (1988) 1804–1826.

[22] Y.K. Yong, M.G. Nour, E.G. Nawy, Behavior of laterally confined high-strength concrete under axial loads, J Struct Eng 114 (2) (1988) 332–351.

[23] L.P. Saenz, Equation for the stress-strain curve of concrete, ACI J 61 (9) (1964) 1229–1235.

[24] G. Asran, H. EL-Esnawi, S. Fayed, Numerical Investigation of RC Exterior Beam Colum Connections under Monotonic Loads, J Mech Civ Eng 13 (1) (2016) 60–67.

[25] H.T. Hu, W.C. Schnobrich, Constitutive modeling of concrete by using nonassociated plasticity, J Mater Civ Eng 1 (4) (1989) 199–216.

[26] A.M. Sharif, M.A. Samaaneh, A.K. Azad, M.H. Baluch, Use of CFRP to maintain composite action for continuous steel-concrete composite girders, J Compos Constr 20 (4) (2015).

[27] ACI. Building Code Requirements for Structural Concrete. Committee report 318–08, American Concrete Institute, Detroit, Michigan; 2018; p. 473.

[28] N. Elmezaini, M. Ashour, Nonlinear analysis of concrete beams strengthened with steel fiber-reinforced concrete layer, J Eng Res Technol 2 (3) (2015) 181–188.

[29] P.K. Mallick, Fiber-reinforced composites, Marcel Dekker, New York, 1993.

[30] A. Ghobarah, A. Biddah, M. Mahgoub, Rehabilitation of reinforced concrete columns using corrugated steel jacketing, J Earthquake Eng 1 (4) (1997) 651–673.

[31] Sadone R, Quiertant M, Mercier J, Ferrier E. Experimental Study on RC Columns Retrofitted by FRP and Subjected to Seismic Loading. In 6th International conference on FRP composites in civil engineering CICE, Rome, Italy; 2012.

[32] Al-Salloum YA, Al-Sayed SH, Al-Musallam TH, Siddiqui NA. seismic performance of shear deficient exterior RC beam-column joints repaired using CFRP composites. Saudi engineering conference; 2002.